Chinese Chemical Letters 32 (2021) 2017–2020

Contents lists available at ScienceDirect

Chinese Chemical Letters

journal homepage: www.elsevier.com/locate/cclet

Communication

Porous Ni/NiO nanohybrids for electrochemical catalytic glucose oxidation

Jiawei Gu[a], Yuxia Xu[b], Qing Li[a,b,*], Huan Pang[a,*]

[a] School of Chemistry and Chemical Engineering, Yangzhou University, Yangzhou 225009, China
[b] Guangling College, Yangzhou University, Yangzhou 225009, China

ARTICLE INFO

Article history:
Received 29 October 2020
Received in revised form 25 November 2020
Accepted 30 November 2020
Available online 4 December 2020

Keywords:
Porous
Ni/NiO
Nanohybrids
Electrocatalysis
Glucose

ABSTRACT

The remarkable development of nanotechnology and nanoscience has greatly promoted the vigorous development of the field of nanomaterials. This study explores a porous cuboid Ni/NiO composite nanomaterial obtained by calcining $NiC_2O_4{\cdot}2H_2O$ under a N_2 environment. The composite affords direct electrochemical activity and good electrocatalytic properties. Compared to uncalcined precursor, the porous Ni/NiO obtained after calcination exhibited higher catalytic activity for glucose oxidation with higher sensitivity. Moreover, because of its regular cube structure the as-synthesized Ni/NiO exhibited improved electrochemical stability. Such porous Ni/NiO nanocubes represent promising glucose catalyst with high sensitivity and selectivity, improved stability and fast amperometric response.

Over the past few decades, researchers have made several attempts to prepare highly reactive catalysts, such as nickel-based alloys [1], nitrides [2,3], phosphates [4,5] and metal-organic frameworks (MOFs) [6,7]. Porous materials (MOFs and their derivatives) [8–11] and hybrid materials (metal-based heterogeneous materials) [12–15] have been reported widely. With the continuous development of porous materials in the field of electrochemical catalysis, porous hybrid materials (such as nickel-cobalt-based nanomaterials) have gained prominence owing to their larger specific surface area and numerous active sites. These hybrids have been widely used in the field of electrochemical catalysis as they promote electron transfer and ion diffusion and exhibit superior electrochemical activity.

The synthesis of porous hybrid materials by the calcination of complexes or MOF precursors is a promising method. At the same time, calcination of oxalate to obtain porous materials is also a good choice. A nickel oxalate precursor is calcined under nitrogen to form a compound with a unique structure, and these materials have become a class of potentially valuable materials [16–19] that are widely used in electrosensing and electrochemical energy storage. Zhu *et al.* studied the application of porous heterojunction materials in the field of electrical sensing [20–22]. Porous structures are also beneficial for energy storage. Zou *et al.* proposed an in-situ growth method for the preparation of ultrathin nano-nickel hydroxide tablets with a vertical embedded thickness of 1.5 nm, the three-dimensional ordered porous structure of NiFe nanosheet nickel hydroxide can provide effective electrocatalytic performance [23]. Liu *et al.* studied the new three-dimensional mixed structure of porous cobalt nanoribbon@ultrathin nickel hydroxide (NiHON) directly grown on the nanoscale with high porosity and high specific surface area, and obtained high electrochemical activity [24]. Thus, porous hybrids are suitable materials for catalytic reactions.

At present, the electrocatalytic glucose oxidation reaction (GOR) has become an important research direction in the field of electrocatalysts, due to its broad application prospects (in biofuel cells, glucose sensors, implantable fuel cells, *etc.*) [25–27]. Through years of research and exploration by many researchers, the field of GOR research has been continuously progressed, especially in finding new materials to effectively catalyze glucose. Recently, nickel-based nanomaterials were shown to be effective glucose oxidation catalysts [28–30]. The disadvantage of nickel nanoparticles as catalysts is that they are magnetic and easily agglomerate. However, NiO prepared by calcining does not readily aggregate and has no magnetism, but its conductivity is poor [31–33]. Therefore, fabrication of a Ni/NiO nanohybrid is an effective way to obtain a high-performance glucose oxidation catalyst. For example, Sun *et al.* constructed a non-enzymatic glucose electrochemical sensor based on a Ni metal-organic skeleton (MOF)/Ni/NiO nanocomposite modified with gold nanoparticles [34]. Therefore, designing a Ni/NiO nanohybrid as a glucose catalyst is promising.

* Corresponding authors at: School of Chemistry and Chemical Engineering, Yangzhou University, Yangzhou 225009, China.
E-mail addresses: lq87852976@126.com (Q. Li), panghuan@yzu.edu.cn (H. Pang).

https://doi.org/10.1016/j.cclet.2020.11.066
1001-8417/

Herein, rod-like $NiC_2O_4{\cdot}2H_2O$ is synthesized by alcohol-assisted stirring at a low temperature (60 °C). The $NiC_2O_4{\cdot}2H_2O$ precursor was placed in a tube furnace and the air was purged before heating by flushing the furnace with N_2 at a flow rate of 30 mL/min. Thereafter, under N_2 flow, the material was heated to the target temperature of 400 °C (G2) at 1 °C/min over 2 h. Finally, the product was removed from the furnace. For comparison, two other samples were prepared by controlled annealing at 350 °C (G1) and 400 °C (G3), respectively. Due to its unique porous structure and the existence of nickel nanoparticles, the material has some advantages such as catalytically active sites, easy diffusion of the electrolyte, and easy electron transfer. We proved that this material has good stability and high catalytic activity to catalyze glucose in an electrochemical catalysis experiment, affording a better catalytic effect than other materials. This material may prospectively be extended to the fabrication of glucose sensors for a wider range of applications.

Three Ni/NiO samples (G1-G3) were obtained by calcining the precursor $NiC_2O_4{\cdot}2H_2O$ at different temperatures. The phase purity and crystal structure of the samples was determined by X-ray diffraction (XRD). As shown in Fig. S1 (Supporting informatoin), the precursor was $NiC_2O_4{\cdot}2H_2O$, and its crystal structure was consistent with PDF #21-0297. The thermogravimetric (TG) curve in Fig. S2 (Supporting informatoin) was used to optimize the annealing temperature of the precursor. Fig. S3 (Supporting informatoin) shows the XRD patterns of the three samples, demonstrating that they have similar compositions, all of which were Ni/NiO composites. From the peaks of Ni and NiO, the higher the calcination temperature, the more obvious the peak of NiO, while the peak of Ni becomes smaller. Morphological characteristics of sample G2 are determined by scanning electron microscopy (SEM), transmission electron microscopy (TEM), and energy-dispersive X-ray (EDX) spectroscopy, as shown in Fig. 1. The SEM image (Fig. 1a) and TEM image (Fig. 1b) showed a porous cuboid morphology. Fig. S4 (Supporting informatoin) shows that the surface of the precursor is smooth, and the morphology of samples G1 and G3 are similar to the porous structure of sample G2. Because the morphology of sample G1 is not uniform enough, and the morphology of G3 grows and collapses a bit, sample G2 is selected. HRTEM and EDX (Fig. 1c) were used to further analyze the distribution of Ni and O in the composites, demonstrating uniform distribution of these elements. High resolution transmission electron microscope (HRTEM) image in Fig. 1d shows that the interplanar spacings of the sample of N-340 are ≈ 0.203, 0.241 nm which represent the (111), (101) lattice planes of Ni and NiO, respectively [19]. X-ray photoelectron spectroscopy was used to further study the electronic states of the elements on the sample surface. As shown in Fig. S5 (Supporting informatoin), Ni and O are found in the three samples, and it was also confirmed that the elements were in the same oxidation states in the three samples, confirming their similar composition. In addition, the atomic ratio results of Ni and O are shown in Table S1 (Supporting informatoin), and the XPS peak values of the percentages of Ni(0) and Ni(II) are calculated by Ni 2p, as shown in Table S2 (Supporting informatoin). It can be speculated that the different phases may be one of the reasons for the good catalytic performance. The peaks at 855.1 eV, 851.8 eV are caused by Ni $2p_{3/2}$, and the peak at 872.3 eV is caused by Ni $2p_{1/2}$. Hence, Ni^{2+}, Ni^0 exist in the three samples which are from NiO and Ni, consistent with the result of XRD (Fig. S6 in Supporting informatoin). As shown in Fig. S7 (Supporting informatoin), the peak at 530.7 eV is caused by O 1s.

In order to test the electrochemical performance of samples G1, G2 and G3 in the GOR, a series of electrochemical tests were conducted with a three-electrode system. Cyclic voltammetry was generally used to detect GOR signals. As shown in Fig. 2a, in alkaline environment (0.1 mol/L NaOH), increasing concentrations of glucose (GLU; 0–100 μL) led to stronger current response signals, which shows that G2 supported on a glassy carbon electrode (GCE) can catalyze the GOR. In contrast, the current response signal of G1/GCE and G3/GCE, indicated by S8 and S9 in the figures, are not as strong as the current signal of G2/GCE. Various redox rods appeared within the range of 0.2–0.7 V, indicating that the electrocatalytic process occurred at the center of Ni.

In order to determine the optimal GOR voltage of the sample in the presence of 100 μmol/L GLU, the potential was varied (0.4,

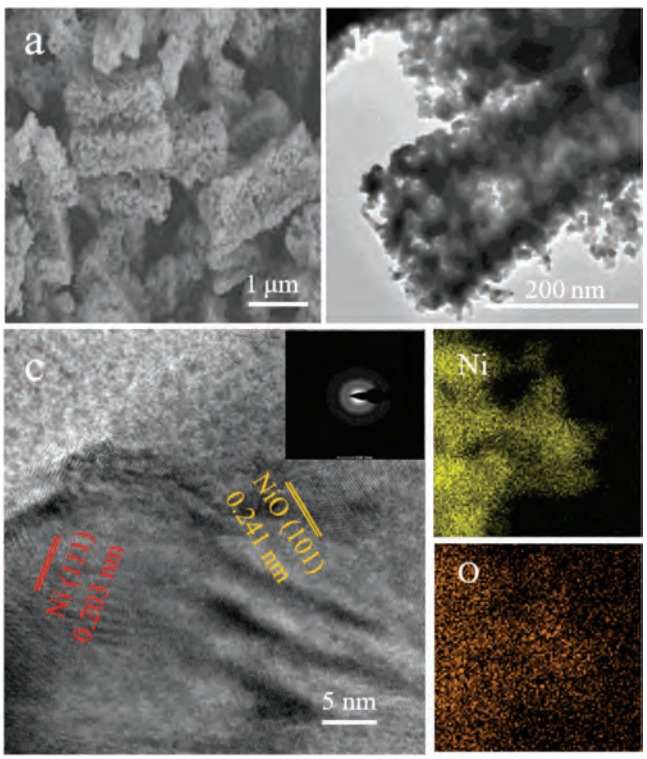

Fig. 1. Morphological characterization of G2. (a) SEM images and (b, c) TEM image and EDX elemental mapping.

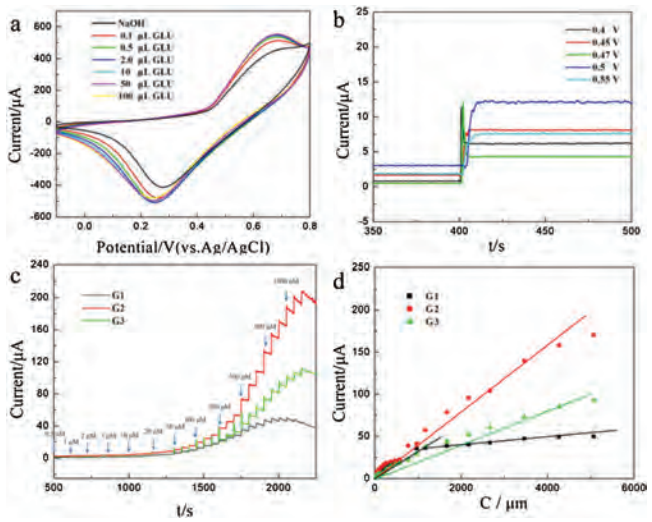

Fig. 2. (a) CV curves of the G2/GCE electrodes with different concentrations of GLU in 0.1 mol/L NaOH. (b) The *i-t* curve of the response of G2/GCE at different potentials. (c) The *i-t* curves of the response of G1/GCE and G2/GCE and G3/GCE with successive additions of GLU in 0.1 mol/L NaOH at 0.45 V. (d) Corresponding calibration *i-c* curves of the response of three samples.

0.45, 0.47, 0.5 and 0.55 V) and the current-time response for sample G2 in 0.1 mol/L NaOH (Fig. 2b) was monitored. When the voltage was too high (0.55 V), the current response was strong but unstable. When the voltage was too low (0.4 V), there was little current response. As shown in Fig. 2b, the stability and sensitivity at these voltages aree not better than those obtained at 0.45 V, and the current signal is clearly improved at 0.4 V. According to the aforementioned analysis, the optimal voltage for the GOR is 0.45 V.

Classic three-electrode system for conduction related GOR electrochemical tests were used to verify the various electrocatalytic performance of these target samples. When using the precursor to test the GOR, the performance was not satisfactory (Fig. S10 in Support information). Fig. 2c shows the current-time (*i-t*) curves of G1/GCE, G2/GCE and G3/GCE after adding GLU (0.1 mol/L NaOH, 0.45 V). During the experiment, at uniform intervals, GLU was dropped into the NaOH solution and stirred evenly; the current signal of the sample gradually increased, and G2 produced a significantly stronger enhancement of the signal intensity. This may be due to the integrity of the G2 form and the homogeneity of the pores, which can provide an abundance of active sites in the GOR, especially if the current response signals of the other two samples change little at high concentrations of GLU. Fig. 2d shows the calibration *i-c* curves of the three samples (Ni/NiO). The three samples showed linear regions between 0.5 mmol/L and 8065.5 mmol/L. The results showed that G2/GCE provided a better linear relationship than G1/GCE and G3/GCE. G2/GCE afforded a wider concentration range and better sensitivity than G1/GCE and G3/GCE, and the catalytic performance was also better for G2/GCE. The linear equations for the three samples within this concentration range can be summarized as follows: (G1) I (μA) = 2.49 + 3.17 × 10^{-2} C_{GLU} (μmol/L), R = 0.9806 (0–1200 μmol/L), sensitivity = 44.87 μA L $mmol^{-1}$ cm^{-2} and I (μA) = 33.88 + 3.11 × 10^{-3} C_{GLU} (μmol/L), R = 0.949 (1200–8065.5 mmol/L, sensitivity = 44.02 μA L $mmol^{-1}$ cm^{-2}); (G2) I (μA) = 5.47 + 3.81 × 10^{-2} C_{GLU} (μmol/L) (R = 0.9958, sensitivity = 53.93 μA L $mmol^{-1}$ cm^{-2}); (G3) I (μA) = 3.509 + 2.09 × 10^{-2} C_{GLU} (μmol/L), R = 0.9899, sensitivity = 29.58 μA L $mmol^{-1}$ cm^{-2}. G2/GCE provided a good linear relationship over a wide range of concentrations, plausibly due to its unique porous structure. Table S1 lists the performance of other materials as GLU catalysts, and the results further confirm that the materials synthesized in this study are very promising GLU catalysts.

The repeatability, stability and anti-interference were also indispensable parameters for assessing the performance of electrodes. The effect of various possible interferents (dopamine, uric acid, ascorbic acid, NaCl) on the GOR was evaluated. As shown in Fig. 3a, the current signal is largely unaffected by these compounds, which indicates that the three electrodes have strong anti-interference ability. Specifically, the current signal of G2/GCE was more responsive than that of the other two. Fig. 3b shows that these three samples provide repeatable performance. As expected, the repeatability of the sample is better, especially for the G2/GCE electrode. It may be due to the regular cubic structure of the sample. In the stability tests (Fig. 3c), the three electrodes performed well with a cycle time of 4000 s. To illustrate the electron transfer capacity of the three nickel oxides, the electrochemical impedance spectroscopy (EIS) response was monitored at 0.45 V for G1/GCE, G2/GCE, G3/GCE and bare GCE in 0.1 mol/L NaOH. As shown in Fig. 3d, G2/GCE had a lower EIS response than G1/GCE and G3/GCE, which proves that the porous cuboid has faster charge transfer capability.

The aforementioned results indicate that Ni/NiO has good electrochemical properties. We also studied the stability of sample G2 from other aspects. SEM images were acquired after immersing G2 in 1 mol/L NaOH for 2, 4 and 6 h (Figs. 4a-c). The overall morphology was roughly unchanged after this process,

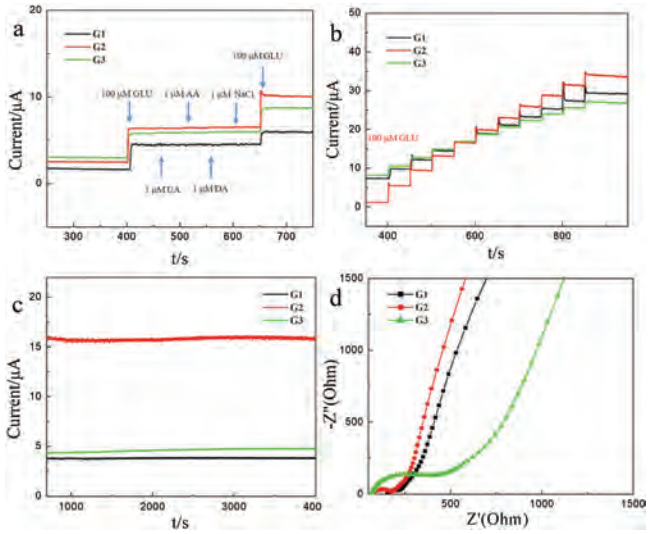

Fig. 3. (a) Current response curves of G1/GCE, G2/GCE and G3/GCE among various interference factors. (b) The *i-t* response of the three samples with the addition of 100 μmol/L GLU ten times into 0.1 mol/L NaOH at 0.45 V. (c) Stability response of three samples in 0.1 mol/L NaOH at 0.45 V. (d) The EIS response of G1/GCE, G2/GCE and G3/GCE in 0.1 mol/L NaOH at 0.45 V.

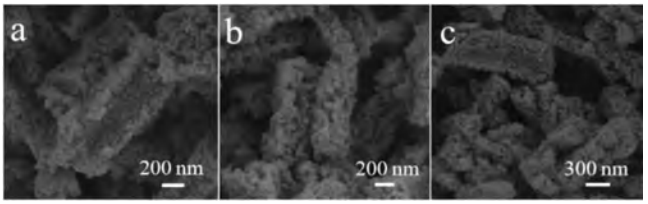

Fig. 4. The SEM images of G2 dipped in 1 mol/L NaOH for (a) 2, (b) 4 and (c) 6 h.

demonstrating the stability of sample G2. These results are also consistent with electrochemical test results. In conclusion, the excellent electrochemical performance of G2 may be derived from many factors. The porous cuboid structure affords a number of advantages-catalytically active sites, easy diffusion of the electrolyte, and easy electron transfer. In most cases, the porous structure shortens the path between particles and speeds up their migration.

In conclusion, a simple and scalable method was used to prepare three Ni/NiO electrodes for the GOR by varying the calcination temperature. The successful synthesis of this material can further advance the utilization of the GOR by providing effective catalysts. Further research should focus on catalyzing glucose reactions more effectively and solving a series of problems that arise in the process of catalyzing glucose oxidation. As expected, the Ni/NiO electrode with a porous cuboid structure (thickness: approximately 2.3 nm) afforded higher electrocatalytic activity, excellent selectivity, and easy electron transfer. Our research will be extended to multi-metal oxide electrocatalysts to achieve improved performance in electrocatalytic applications.

Declaration of competing interest

The authors declare that they have no known competing financial interests or personal relationships that could have appeared to influence the work reported in this paper.

Acknowledgments

This work was supported by the National Natural Science Foundation of China (NSFC, Nos. U1904215 and 21671170), and the

Top-notch Academic Programs Project of Jiangsu Higher Education Institutions (TAPP). Program for Young Changjiang Scholars of the Ministry of Education, China (No. Q2018270). We also acknowledge the Priority Academic Program Development of Jiangsu Higher Education Institutions.

Appendix A. Supplementary data

Supplementary material related to this article can be found, in the online version, at doi:https://doi.org/10.1016/j.cclet.2020.11.066.

References

[1] C. Cheng, S.S.A. Shah, T. Najam, et al., Energy Chem. 26 (2017) 1245–1251.
[2] A.M. Alexander, J.S.J. Hargreaves, Chem. Soc. Rev. 39 (2010) 4388.
[3] Y. Wang, Q. Li, W. Shi, P. Cheng, Chin. Chem. Lett. 31 (2020) 1768–1772.
[4] J.S. Moon, J.H. Jang, E.G. Kim, et al., J. Catal. 326 (2015) 92–99.
[5] L. Feng, H. Vrubel, M. Bensimon, X. Hu, Phys. Chem. Chem. Phys. 16 (2014) 5917.
[6] K. Cao, L. Jiao, H. Xu, et al., Adv. Sci. 3 (2016) 1500185.
[7] C. Wei, C. Cheng, J. Zhao, et al., Chem. Open 4 (2015) 32–38.
[8] N. Zhang, L. Yan, Y. Lu, et al., Chin. Chem. Lett. 31 (2020) 2071–2076.
[9] M. Yuan, H. Zhang, C. Yang, F. Wang, Z. Dong, ChemCatChem 11 (2019) 3327–3338.
[10] X. Li, X. Yang, H. Xue, H. Pang, Q. Xu, Energy Chem. 2 (2020) 100027.
[11] D. Zhang, P. Wang, F. Chen, et al., Chin. Chem. Lett. 31 (2020) 2795–2798.
[12] Q. Yang, G. Li, K. Manna, et al., Adv. Mater. 32 (2020) 1908518.
[13] X. Li, X. Yang, Y. Huang, T. Zhang, B. Liu, Adv. Mater. 31 (2019) 1902031.
[14] L. Jin, H. Pang, Chin. Chem. Lett. 31 (2020) 2300–2304.
[15] Y. Lu, T. Wang, X. Li, et al., RSC Adv. 6 (2016) 87188–87212.
[16] L. Jiao, Y. Wang, H.L. Jiang, Q. Xu, Adv. Mater. 30 (2018) 1703663.
[17] X. Wang, Y. Li, T. Jin, et al., Nano Lett. 17 (2017) 7989–7994.
[18] X. Xiao, Q. Li, X. Yuan, et al., Small Methods 2 (2018) 1800240.
[19] Q. Li, N. Li, J. An, H. Pang, Inorg. Chem. Front. 7 (2020) 2089–2096.
[20] P.P. Li, Y. Cao, C.J. Mao, B.K. Jin, J.J. Zhu, Anal. Chem. 91 (2019) 1563–1570.
[21] Y. Chen, D. Zhao, J. Fu, et al., Anal. Chem. 91 (2019) 6829–6835.
[22] X. Sheng, D. He, J. Yang, K. Zhu, X. Feng, Nano Lett. 14 (2014) 1848–1852.
[23] X. Li, D. Ma, C. Cao, et al., Small 15 (2019) 1902218.
[24] C. Guan, J. Liu, C. Cheng, et al., Energy Environ. Sci. 4 (2011) 4496.
[25] K. Shim, W.C. Lee, Y.U. Heo, et al., Sci. Rep. 9 (2019) 894.
[26] Y. Qin, Y. Sun, Y. Li, C. Li, L. Wang, Chin. Chem. Lett. 31 (2020) 774–778.
[27] A.J. Gross, X. Chen, F. Giroud, et al., ACS Catal. 7 (2017) 4408–4416.
[28] Z. Ren, H. Mao, H. Luo, X. Deng, Y. Liu, Nanotechnology 31 (2020) 185501.
[29] H.L. Hu, C. He, B.G. Guo, et al., Nanosci. Nanotechnol. 20 (2020) 3246–3251.
[30] H. Yin, T. Zhan, J. Chen, et al., J. Mater. Sci. Mater. Electron. 31 (2020) 4323–4335.
[31] H. Lai, Q. Wu, J. Zhao, et al., Energy Environ. Sci. 9 (2016) 2053–2060.
[32] B.S. Batule, K.S. Park, S. Gautam, et al., Sens. Actuator. B: Chem. 283 (2019) 749–754.
[33] P. Chakraborty, S. Dhar, K. Debnath, T. Majumder, S.P. Mondal, Sens. Actuator. B: Chem. 283 (2019) 776–785.
[34] J. Chen, Q. Xu, Y. Shu, X. Hu, Talanta 184 (2018) 136–142.